An Upflow Microbial Fuel Cell with an Interior Cathode: Assessment of the Internal Resistance by Impedance Spectroscopy †

ARTICLE *in* ENVIRONMENTAL SCIENCE AND TECHNOLOGY · OCTOBER 2006

Impact Factor: 5.33 · DOI: 10.1021/es060394f · Source: PubMed

4 AUTHORS, INCLUDING:

Zhen (Jason) He
Virginia Polytechnic Institute and State Univ…
106 PUBLICATIONS **3,488** CITATIONS
SEE PROFILE

Shelley Minteer
University of Utah
243 PUBLICATIONS **4,553** CITATIONS
SEE PROFILE

Largus Angenent
Cornell University
137 PUBLICATIONS **5,327** CITATIONS
SEE PROFILE

Environ. Sci. Technol. **2006**, *40,* 5212−5217

An Upflow Microbial Fuel Cell with an Interior Cathode: Assessment of the Internal Resistance by Impedance Spectroscopy†

ZHEN HE,‡ NORBERT WAGNER,§ SHELLEY D. MINTEER,|| AND LARGUS T. ANGENENT*,‡

Department of Chemical Engineering and Environmental Engineering Science Program, Washington University in St. Louis, St. Louis, Missouri 63130, Institute for Technical Thermodynamics, German Aerospace Center, D-70569 Stuttgart, Germany, and Department of Chemistry, Saint Louis University, St. Louis, Missouri 63103

An upflow microbial fuel cell (UMFC) system with a U-shaped cathode inside the anode chamber was developed and produced a maximum volumetric power of 29.2 W/m^3 at a volumetric loading rate of 3.40 kg COD/(m^3 day) and an operating temperature of 35 °C while feeding sucrose continuously. The Coulombic efficiency decreased from 51.0% to 10.6% with the increase in the volumetric loading rate from 0.57 to 4.29 kg COD/(m^3 day). In addition, the lab-scale UMFC maintained soluble chemical oxygen demand (COD) removal efficiencies exceeding 90% and volatile fatty acid concentrations of ∼40 mg/L, indicating efficient wastewater treatment. The analysis of impedance spectroscopy, generated by fitting experimental data into an equivalent circuit, revealed that at a volumetric loading rate of 3.40 kg COD/(m^3 day) the overall internal resistance was 17.13 Ω. This internal resistance was composed of electrolyte resistance (8.62 Ω), charge-transfer resistance (7.05 Ω), and diffusion resistance (1.46 Ω). Electrolyte resistance dominated throughout the entire range of loading rates. In addition, impedance spectroscopy demonstrated that both the anodic and the cathodic charge-transfer resistances were important limiting factors. To further improve the power output of the UMFC, we must reduce the electrolyte resistance by optimizing reactor configuration, reduce the anode charge-transfer resistances by selecting superior anodic microbiota, and reduce the cathodic charge-transfer resistance by exploring sustainable and efficient catalysts.

Introduction

The electrochemical limitations on the performance of microbial fuel cells (MFCs) are due to the internal resistance (R_i), which results from ohmic, kinetic, and transport limitations (*1*, *2*). For MFCs, ohmic limitation is mostly due to the resistance of electrolytes, such as anolyte, catholyte, and proton exchange membrane (PEM), while kinetic limitation is a charge-transfer resistance due to slow activation reaction rates on anode and cathode electrodes, and transport limitation is a resistance caused by retarded diffusion. A reverse correlation exists between R_i and power output, and researchers, therefore, have attempted to reduce R_i by optimizing reactor configurations and cathode catalysts/mediators without losing practicality (*3*−*5*).

Correct measurement and assessment of R_i for a MFC will help researchers understand the limitations of their systems and boost power output. Impedance spectroscopy (IS) is a technique that measures the resistance of an electric circuit to current flow, which is expressed as R_i (*6*). This technique can provide detailed information on the relative contribution of different components to R_i in an electrochemical cell (*7*). Researchers have utilized IS to characterize the electrochemical kinetics of anodic and cathodic processes in enzyme-driven biofuel cells and found that the cathodic biocatalytic process was the main contributor to the overall electron-transfer resistance (*8*). No information on the electrolyte resistance was available from this study, probably due to its negligible quantity in such biofuel cells. However, the electrolyte resistance plays an important role in MFCs, because ion transport in electrolytes was affected by reactor configuration and fuel composition (*4*). To our knowledge, IS has not been performed in detail with MFCs.

Microbial fuel cells achieve a comparable organic removal efficiency to current biological wastewater treatment processes, such as anaerobic digesters (*1*, *9*−*13*). To compete with anaerobic digesters for electricity production after conversion of methane gas to electricity via a generator, however, MFCs must produce a volumetric power up to 160 W/m^3 (based on the wet volume of the anode chamber) (*1*). To date, a maximum volumetric power of 216 W/m^3 was produced from a MFC with an anode wet volume of 40 mL (*9*). A sensor-type MFC with a volume of 20 mL also obtained a high power output of 102 W/m^3 (*13*). Thus, MFCs have considerable potential as wastewater treatment systems while simultaneously generating electricity (*14*, *15*). Besides satisfying organic removal efficiency and power output, a practical reactor configuration must be developed that can be economically scaled up.

Microbial fuel cells with a flow pattern through a porous anode electrode are advantageous, because contact between substrate and biomass is made by the influent flow rather than mechanical mixing (*1*, *2*). We have used such a flow pattern in an upflow microbial fuel cell (UMFC) (*1*). In addition to a practical configuration, UMFCs achieved promising power outputs. Recently, an UMFC (or tubular MFC) with a wet anode volume of 210 mL generated a maximum volumetric power of 90 W/m^3 during continuous treatment of acetate (*2*). This UMFC was configured with an exterior cathode over which hexacyanoferrate (catholyte) was recirculated. The anode consisted of graphite granules through which acetate flowed. A relatively low R_i of 4 Ω was achieved by sustaining a short distance between the anode and cathode electrodes and a large PEM surface area (*2*). However, scaleup of this UMFC with an exterior cathode would considerably increase the volume to surface area ratio and thus increase the electrode distance and decrease the relative PEM surface area, resulting in a higher R_i and a lower power output.

Here, we describe electricity generation from sucrose solution by an UMFC with the cathode chamber placed inside the anode chamber. Such an interior cathode had been studied previously with a horizontal-flow MFC (*10*). The

* Corresponding author phone: (314) 935-5663; fax: (314) 935-5464; e-mail: angenent@seas.wustl.edu.

† This article is part of the Microbial Fuel Cells Focus Group.

‡ Washington University in St. Louis.
§ German Aerospace Center.
|| Saint Louis University.

10.1021/es060394f CCC: $33.50
Published on Web 06/29/2006

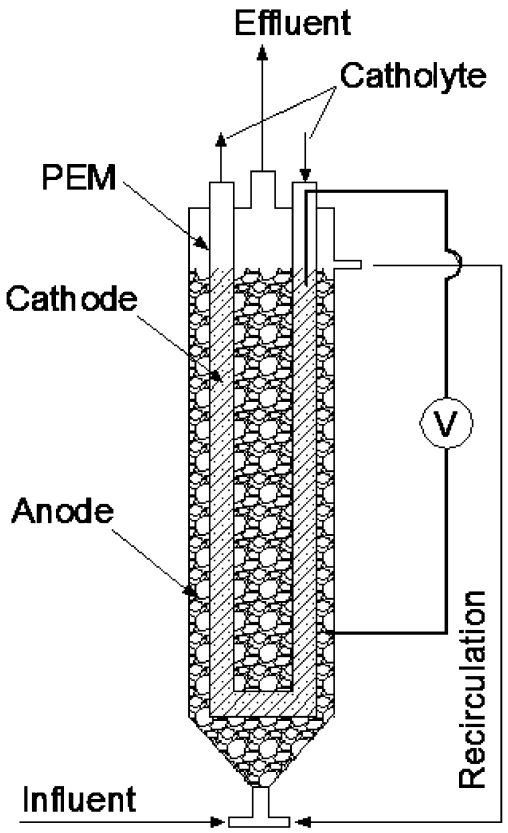

FIGURE 1. Lab-scale $UMFC_1$ with an interior cathode.

anode electrode volume of the UMFC was sufficiently utilized, ensuring a low volume to PEM surface area ratio even during scaleup. We compared R_i and power output of this UMFC with our other UMFC configurations to investigate the advantages of an interior cathode system. In addition, IS was applied to distinguish between resistances of electrolyte, charge transfer, and other possible components.

Materials and Methods

UMFC Setup. A U-shaped cathode compartment with a 2 cm diameter was constructed by gluing two tubes made from PEM (Ultrex CMI-7000, Membrane International, Inc., Glen Rock, NJ; a total surface area of 188 cm^2) into a plastic base connector. The cathode was installed inside the anode chamber ("$UMFC_1$", Figure 1). Both the anode and the cathode chambers were then filled with granular activated carbon (General Carbon Corporation, Paterson, NJ). The total and wet volumes were 440 and 180 cm^3 for the anode chamber, and 210 and 90 cm^3 for the cathode chamber, respectively. A copper wire was connected to both a graphite rod (Poco Graphite, Inc., Decatur, TX) in the anode chamber and a carbon fiber (Zoltek Companies, Inc., St. Louis, MO) in the cathode chamber to form an external circuit. To investigate the effect of reactor configuration on R_i, we modified a previously described UMFC (*1*) by replacing the reticulated vitreous carbon (RVC) cathode with platinum-coated carbon paper (P50, Ballard Material Products, Inc., Lowell, MA) and maintaining all other conditions the same. The modified UMFC was assigned "$UMFC_2$", while the unmodified system was designated here as "$UMFC_3$". Both $UMFC_2$ and $UMFC_3$ contained the cathode chamber on the top of the anode chamber (*1*). We used Masterflex pumps (Cole-Parmer Instrument Company, Vernon Hill, IL) for feeding and recirculation and a milligascounter (Calibrated Instruments, Inc., Hawthorne, NY) for biogas measurement.

Operating Conditions. Granular anaerobic sludge from a mesophilic upflow anaerobic bioreactor treating brewery wastewater was used to inoculate the UMFCs. Before inoculation, the sludge was ground with a mortar and pestle and then filtered through a 0.25 mm pore size sieve to remove large particles. The sucrose solution consisted of (per liter of deionized water) sucrose, 0.125−0.833 g; NH_4Cl, 0.03 g; $CaCl_2 \cdot 2H_2O$, 0.30 g; KCl, 0.66 g; NaCl, 0.60 g; $MgCl_2$, 6.30 g; K_2HPO_4, 2.00−8.00 g; KH_2PO_4, 4.50−18.00 g; $FeCl_2$, 0.03 g; $MgSO_4$, 0.006 g; iron citrate, 0.01 g; yeast extract, 0.001−0.003 g; and trace metals (1 mL) (*16*). The operating pH of the anolyte was maintained between 5.8 and 6.3 depending on the external resistor and the phosphate buffer levels in the influent. The sucrose solution was maintained at 4 °C under a nitrogen gas atmosphere. $UMFC_1$ was operated at 35 °C and continuously fed at a flow rate of 0.5 mL/min with a hydraulic retention time (HRT) of 6 h. The volumetric loading rate (based on the wet volume of the anode chamber) was increased from 0.57 to 4.29 kg COD/(m^3 day) by a stepwise increase in the influent chemical oxygen demand (COD) concentration from 142 to 1072 mg/L. During startup and after stepwise increases in the volumetric loading rate, the external resistance (R_e) was set at 100 Ω. After a steady-state voltage was obtained for each of the applied volumetric loading rates, we decreased R_e to 33 Ω to perform chemical and electrochemical analysis. Effluent from the anode chamber was recirculated at a flow rate of 180 mL/min and mixed with influent to maintain an upflow velocity in the anode chamber of 4 m/h. A 100 mM potassium hexacyanoferrate and 100 mM potassium phosphate buffer solution (Sigma-Aldrich, St. Louis, MO) was recirculated in the cathode chamber at a flow rate of 150 mL/min. $UMFC_2$ was operated similarly as $UMFC_3$ according to He et al. (*1*).

Chemical Analysis. The total chemical oxygen demand (COD) in the influent, soluble COD (SCOD), and volatile fatty acid (VFA) levels in the effluent were measured according to procedures described in ref *17*. Triplicate samples from the same reactor were taken during three consecutive days. The composition of the biogas was analyzed using a gas chromatograph (series 350, GOW-MAC, Bethlehem, PA) with a thermal conductivity detector (*1*).

Electrochemical Measurement. The voltage (E) across a resistor (R) was measured by a data acquisition module, and the Coulombic efficiency and energy efficiency were calculated according to ref *1*. The volumetric power was calculated as $P = EI/V$, where V was the wet volume of the anode chamber and I was current. The fill factor (i.e., the ratio of actual maximum power over the theoretical maximum power) of a MFC was evaluated by $f = P_{max}/(I_{sc}E_{op})$, where P_{max} was the maximum power and I_{sc} and E_{oc} were short-circuit current and open potential, respectively (*18*). The polarization curve was constructed by changing R_e from open circuit to 0 Ω. The sustainable volumetric power was determined by varying R_e from 100 to 10 Ω using an ohm-ranger (Ohmite Manufacturing Co., Rolling Meadows, IL) at 1 h and 1 day intervals.

Impedance Spectroscopy. To quantify and analyze R_i, IS was performed with a potentiostat (611B, CH Instruments Inc., Austin, TX) at a frequency range of $1-10^5$ Hz between the anode and the cathode (two-electrode mode), and the experimental spectra were then fit into equivalent circuits according to Wagner (*19*) using potentiostat software (CH Instruments Inc.), generating data from the real part (Z_{re}) and imaginary part (Z_{im}) that are shown in a Nyquist plot (*7*). A Nyquist plot typically consists of a semicircle and a linear portion, which represents electrolyte and charge-transfer resistance and diffusion resistance, respectively (*6*). A slow electron-transfer process, which is anticipated in MFCs, will result in a relatively large semicircle part and a relatively small or nonexistant linear portion. On the Nyquist plot, the

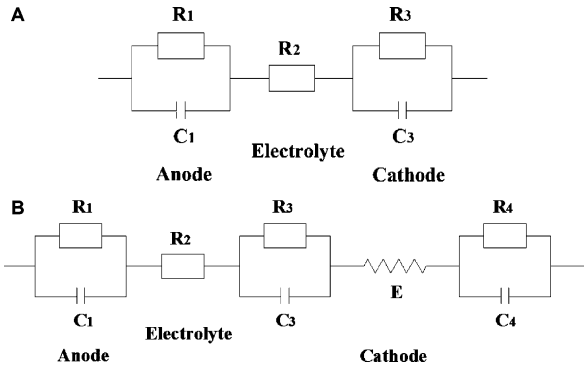

FIGURE 2. Equivalent circuits of UMFC$_1$: (A) two time constants of the anode and cathode; (B) three time constants.

portion in the high-frequency (HF) range (the intercept of the semicircle with the Z_{re} axis) is the electrolyte resistance, while in the low-frequency (LF) range the total R_i (summation of all contributions) can be found (*19*). The difference between HF and LF represents the charge-transfer and diffusion resistances.

Equivalent Circuit. To evaluate the measured impedance data, the reaction components in the UMFC were converted into an equivalent circuit (*19*) (Figure 2). Symbols "R" and "C" represent resistor and capacitor, respectively. A capacitor is formed at the interface between the electrode and its surrounding electrolyte (shown as a double layer) when charges in the electrode are separated from those in the electrolyte (*7*). Symbols R_1 and R_3 are expressed as charge-transfer resistances, related to the activation energy of the anode and cathode; R_2 represents electrolyte resistance, including resistance from the PEM, anolyte, and catholyte (Figure 2A) (*19*). It was experimentally verified whether R_1 or R_3 represented the anode or the cathode. The equivalent circuit in Figure 2A is modified by replacing capacitor components with constant phase elements (CPE, still using symbol "C") (Figure 2B). A capacitor represents a very smooth electrode surface, while a CPE suggests a rough electrode surface (similar to our electrode). Symbol "E" is the element that represents the contribution of the inductive coupling in the high-frequency range of the wire. A RC term (R_4 and C_4) is a diffusion element, which is used to describe a "finite diffusion" (i.e., diffusion length is small).

Results and Discussion

Electricity Generation. UMFC$_1$ continuously generated electricity from the anaerobic oxidation of sucrose for a period of 4 months at an operating temperature of 35 °C (data not shown). During the first 20 days, UMFC$_1$ was fed at a volumetric loading rate of 2.85 kg COD/(m^3 day) to grow biomass on granular activated carbon in the anode until a stable current was obtained at a 100 Ω R_e. On day 21, the volumetric loading rate was decreased to 0.57 kg COD/(m^3 day) to select for anodophilic microbes. Subsequently, R_e was changed to 33 Ω on day 26 to achieve a higher power output throughout chemical and electrochemical analyses. During stepwise increases in the loading rate from 0.57 to 3.40 kg COD/(m^3 day), the volumetric power increased from 9.70 to 27.2 W/m^3 (R_e = 33 Ω) (Figure 3A). After the loading rate increased further to 4.29 kg COD/(m^3 day), this power decreased to 23.7 W/m^3 due to deteriorating environmental conditions with increased levels of SCOD and VFA intermediates (Figure 3B). Clearly, the loading rate of 4.29 kg COD/(m^3 day) was beyond the electricity-conversion capacity of UMFC$_1$. The Coulombic efficiency (i.e., electron recovery from the total COD fed) of UMFC$_1$ decreased from 51.0% to 10.6% with increasing loading rates (R_e = 33 Ω), indicating that the

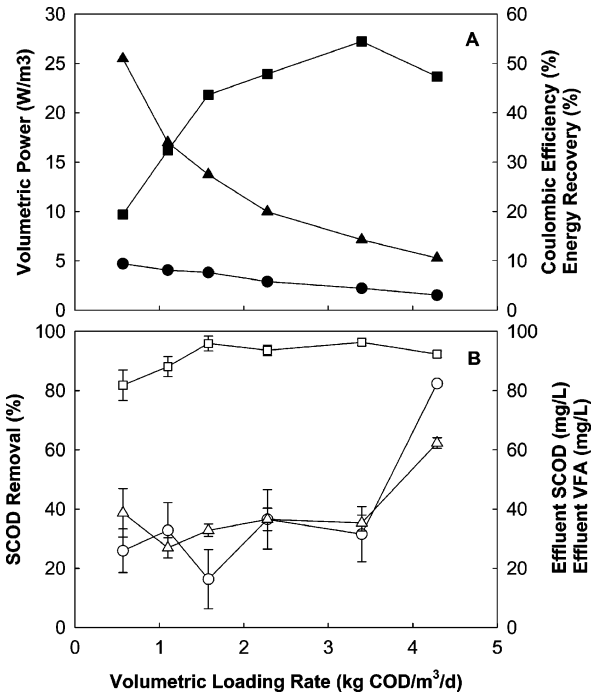

FIGURE 3. Performance of UMFC$_1$ at an external resistance of 33 Ω at different volumetric loading rates: (A) volumetric power (■), Coulombic efficiency (▲) and energy recovery (●); (B) SCOD removal efficiency (□), effluent VFA level (△), and SCOD concentration (○). Bars represent standard deviations based on triplicate measurements from a single reactor.

electricity-conversion capacity did not improve linearly with the increase in loading rates (Figure 3A). Meanwhile, the energy recovery from sucrose fed to UMFC$_1$ decreased from 10% to 3% (R_e = 33 Ω). These values were similar compared to Liu et al. (*20*). Some caution must be taken into consideration with such a direct comparison, because the latter study used acetate/butyrate at an operating temperature of 30 °C and we used sucrose as the electron donor at 35 °C. We anticipated a considerably lower energy recovery for sucrose than acetate due to a more elaborate degradation pathway for sucrose. A higher operating temperature of 35 °C may explain the similar energy recovery values due to a higher metabolic rate and efficiency.

Organic Removal and Biogas Formation. UMFC$_1$ maintained high organic removal efficiencies exceeding 90% based on SCOD (at a 33 Ω R_e). The concentrations of SCOD and VFA in the effluent were generally <40 mg/L and increased to 82.4 ± 1.1 and 62.3 ± 1.8 mg/L, respectively, when the volumetric loading rate was increased from 3.40 to 4.29 kg COD/(m^3 day) (Figure 3B). Biogas production was observed from UMFC$_1$ during the entire operational period, but the biogas production rate and methane content increased with increasing loading rate. At the lowest loading rate of 0.57 kg COD/(m^3 day), the biogas production was ~8 mL/day with a methane content of 0.2%. The contribution of COD removal by methanogens was negligible, indicating that anodophilic biomass has a competitive advantage over methanogens at the >0 mV anodic potential compared to a standard hydrogen electrode (*21*). When the volumetric loading rate was increased, however, substrates were supplied beyond the electricity-conversion capacity of UMFC$_1$, which resulted in a biogas production of 100 mL/day (containing 56% of methane), corresponding to 26% of the COD fed (at a volumetric loading rate of 3.40 kg COD/(m^3 day) and R_e = 33 Ω). Increased methane production at high loading rates confirmed our previous conclusion that methane gas will be produced in overloaded MFCs (*1*).

TABLE 1. Comparison of Performance of Three Types of UMFCs

UMFC configuration	cathode electron shuttle/catalyst	E_{oc}[a] (V)	I_{sc}[b] (mA)	P_{max}[c] (W/m^3)	R_i[d] (Ω)	reference
$UMFC_1$	hexacyanoferrate	0.65	35.0	29.2 (20 Ω)[e]	17	this study
$UMFC_2$	platinum	0.66	22.0	5.1 (43 Ω)	41	this study
$UMFC_3$	hexacyanoferrate	0.74	9.0	3.1 (66 Ω)	84	*1*

[a] Open potential. [b] Short-circuit current. [c] Maximum volumetric power. [d] Internal resistance. [e] The external resistance where the maximum volumetric power was achieved.

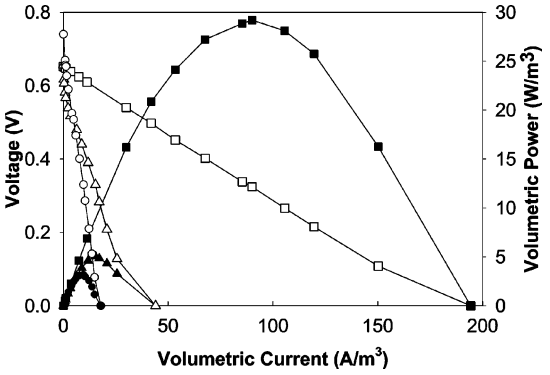

FIGURE 4. Comparison of polarization curves for three UMFCs: $UMFC_1$ (■), $UMFC_2$ (▲), and $UMFC_3$ (●). The blank symbols represent voltage curves.

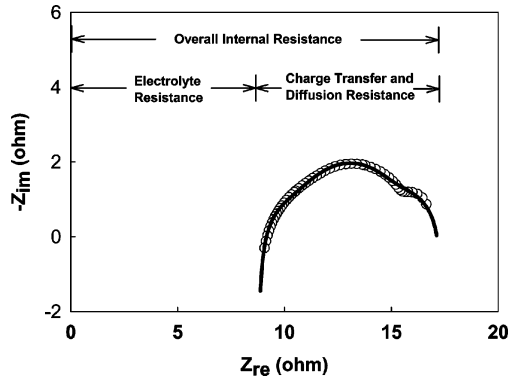

FIGURE 5. Nyquist plots of impedance spectra of $UMFC_1$ at the volumetric loading rate of 3.40 kg COD/(m^3 day): experimental data (circles) measured at open circuit and simulated data (solid line) after fitting to an equivalent circuit (Figure 2B).

Maximum Power Production. The maximum volumetric power of 29.2 W/m^3 was produced from $UMFC_1$ at a volumetric loading rate of 3.40 kg COD/(m^3 day) with a 20 Ω external resistance (R_e) and a 17 Ω internal resistance (R_i) (Figure 4). The sustainable power output from $UMFC_1$, however, was lower than the maximum volumetric power (Supporting Information). In accordance with theory, we obtained the maximum power output when R_e was equivalent to R_i (*8*). The comparison between different reactor configurations showed that $UMFC_1$ with an interior cathode produced a considerably higher power output than $UMFC_2$ and $UMFC_3$ with a cathode on top of the anode (Figure 4). The short-circuit current (indicating the maximum electron recovery) of 35 mA and the maximum volumetric power of 29.2 W/m^3 for $UMFC_1$ were much higher than the values for $UMFC_3$ (9 mA and 3.1 W/m^3, respectively) (Table 1). This corresponded to a lower R_i of 17 Ω for $UMFC_1$ compared to 84 Ω for $UMFC_3$, likely due to reduced ohmic limitations by decreased electrode spacing and increased PEM surface area. Hexacyanoferrate was used for the catholyte in both these UMFCs. To investigate the effect of kinetic limitation in the cathode on power output, we also compared $UMFC_2$ (platinum) and $UMFC_3$ (hexacyanoferrate). The short-circuit current of 22 mA and the maximum volumetric power of 5.1 W/m^3 for $UMFC_2$ were higher than the levels for $UMFC_3$ (Table 1), because of a lower cathodic charge-transfer resistance due to a higher reaction rate with platinum than with hexacyanoferrate. This corresponded to a lower R_i of 41 Ω compared to 84 Ω (Table 1). Our results are different from Oh et al. (*22*), who reported that MFCs with a hexacyanoferrate cathode generated a higher power than MFCs with a platinum cathode. The comparisons between UMFCs indicated that the largest improvement in power output was gained from reducing the ohmic limitations rather than the kinetic limitations.

By analyzing the polarization curve and calculating the fill factor, we suggested that ohmic limitation was still governing the $UMFC_1$ performance despite the improvements that we had made. The shape of the graph for the potential drop in the UMFC polarization curve is linear (Figure 4) and, therefore, fundamentally different from the nonlinear theoretical fuel cell polarization curves. For the latter curves, the kinetic limitation is dominant at low current densities, and transport limitation is found at high current densities while ohmic limitation governs the intermediate region (*23*). A linear curve, however, qualitatively shows the dominance of ohmic limitations. This was also demonstrated by the fill factor, which reflects the deviation of the polarization curve from the theoretical shape. The deviation usually originates from ohmic limitation and/or diffusion resistance. We found a fill factor of 23%, a number that has been linked to ohmic limitations by electrochemists (*18*).

Internal Resistance Analyzed by Impedance Spectroscopy. To obtain quantitative data on the resistances of $UMFC_1$, we analyzed the overall R_i and its sources by fitting experimental data to a hypothetical equivalent circuit that included diffusion resistance (Figure 2B). A Nyquist plot showed that R_i of $UMFC_1$ at the volumetric loading rate of 3.40 kg COD/(m^3 day) was 17.13 Ω (Figure 5). The simulated data in the Nyquist plot (1 Hz to 5 kHz) were generated from the experimental data at the frequency range between 9 Hz and 4.4 kHz. Experimental data at the lowest frequencies (1 to 9 Hz) and the highest frequencies (4.4 to 5 kHz) were not used for our simulation model because of inaccuracies. It was also found that the overall R_i was composed of an electrolyte resistance of 8.62 Ω, a charge-transfer resistance of 7.05 Ω, and a diffusion of 1.46 Ω (Figure 5). The relatively small value of the diffusion resistance showed that transport limitation played a minor role compared to ohmic and kinetic limitations. The impedance test also verified our qualitative analysis suggesting that $UMFC_1$ was still limited foremost by ohmic limitation. With an UMFC using identical PEM material and catholyte, Rabaey et al. (*2*) obtained a lower overall R_i of 4 Ω (and thus a <4 Ω electrolyte resistance) compared to $UMFC_1$. The lower electrolyte resistance in Rabaey et al. (*2*) was likely caused by a higher anolyte conductivity with sodium acetate (up to a concentration of ~780 mg/L) compared to sucrose as an artificial wastewater and a lower volume to PEM surface area ratio of 1.4 compared to 2.3 for $UMFC_1$. This is even more pronounced, because lower electrolyte conductivities exist at an operating temperature

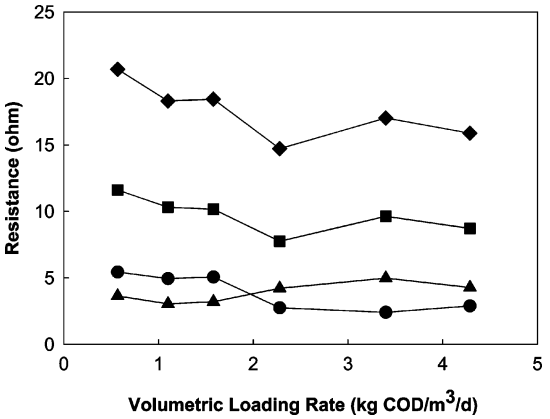

FIGURE 6. Simulated values of overall R_i (sum of R_1, R_2, and R_3, ◆), R_1 (●), R_2 (■), and R_3 (▲) of equivalent circuits without diffusion resistance (Figure 2A) for $UMFC_1$ at different volumetric loading rates, measured at open circuit.

of 25 °C in Rabaey et al. (*2*) compared to those in our study (35 °C).

Charge-transfer resistance, caused by kinetically controlled reactions, can be further characterized as anodic and cathodic charge-transfer resistances. We fitted the IS experimental data of $UMFC_1$ into an equivalent circuit without a diffusion resistance (Figure 2A). The inconsequential diffusion resistance was excluded to simplify the analysis. Experimental data showed that R_1 represented the anode. When the volumetric loading rate was increased from 0.57 to 3.40 kg COD/(m^3 day), R_1 decreased from 5.44 to 2.41 Ω (Figure 6). We found a higher R_1 of 2.89 Ω at a loading rate of 4.29 kg COD/(m^3 day) due to the decreased anodic electricity-conversion ability resulting in lower power output (Figure 3A). Thus, a reverse correlation between anode charge-transfer resistance and power output was observed, indicating the increased electron-transfer ability through the selection of anodophilic microbes. R_3 represented the cathode with a varying resistance between 3.05 and 4.78 Ω over the operating period (the catholyte composition was constant) (Figure 6). From our analysis, we concluded that anode and cathode transfer resistances similarly limited the $UMFC_1$ and that the performance can be further improved by optimizing both the anode and the cathode reaction rates.

The volumetric loading rate was increased by increasing the concentration of sucrose and buffer in the feed while maintaining the nutrients levels constant. The increase in buffer concentration increased the concentration of ions in the anolyte and therefore decreased R_2 from 11.6 to 8.7 Ω over the operating period (the temperature, PEM, and catholyte conductivity were constant). The decrease in R_2 due to increased anolyte conductivity resulted in an overall reduction in R_i (from 20.7 to 15.9 Ω after summation of the individual resistances) with an increasing volumetric loading rate (Figure 6). However, this was not the sole reason for the decline in R_i as the improvement in electron-transfer capability of the anode biomass also affected R_i. This analysis showed that electrolyte resistance dominated over the entire range of volumetric loading rates that were tested.

Implications for Future Studies. Quantification of the components of R_i showed that electrolyte resistance was the major limitation to obtaining a higher power output. Thus, the reactor configuration must be optimized to reduce the ohmic limitations. Further improvements in power can also be made by reducing the relatively large anodic and cathodic kinetic limitations. In the anode, a microbiome with a superior catalytic ability must be selected by optimizing the environmental conditions. In the cathode, the unsustainable hexacyanoferrate must be replaced by a more efficient and suitable compound. The discrepancy in electrochemical behavior between conventional fuel cells and MFCs revealed that specific factors, such as conductivity of the anode and cathode solutions, the presence of biofilms in the anode, and the high activation energy because of the low catalytic ability of microbes, play important roles. Therefore, an electrochemical model must be developed specifically for MFCs to better explain the performance and electrochemical data.

Acknowledgments

We thank Zoltek Companies, Inc. (St. Louis, MO) for donating carbon fibers and Dr. Brian Wrenn (Washington University in St. Louis), Dr. Zhe Lu (Harbin Institute of Technology, People's Republic of China), and anonymous reviewers for helpful comments. We specially appreciate the help from Dr. Eugenii Katz (The Hebrew University of Jerusalem, Israel) with the analysis of impedance spectroscopy. Support for this work was provided by the Bear Cub Fund, Washington University in St. Louis.

Supporting Information Available

Sustainable power production from $UMFC_1$ and the effect of external resistance and pH on current generation. This material is available free of charge via the Internet at http://pubs.acs.org.

Literature Cited

(1) He, Z.; Minteer, S. D.; Angenent, L. T. Electricity generation from artificial wastewater using an upflow microbial fuel cell. *Environ. Sci. Technol.* **2005**, *39*, 5262−5267.

(2) Rabaey, K.; Clauwaert, P.; Aelterman, P.; Verstraete, W. Tubular microbial fuel cells for efficient electricity generation. *Environ. Sci. Technol.* **2005**, *39*, 8077−8082.

(3) Rabaey, K.; Verstraete, W. Microbial fuel cells: Novel biotechnology for energy generation. *Trends Biotechnol.* **2005**, *23*, 291−298.

(4) Liu, H.; Cheng, S.; Logan, B. E. Power generation in fed-batch microbial fuel cells as a function of ionic strength, temperature, and reactor configuration. *Environ. Sci. Technol.* **2005**, *39*, 5488−5493.

(5) Cheng, S.; Liu, H.; Logan, B. E. Power densities using different cathode catalysts (Pt and CoTMPP) and polymer binders (Nafion and PTFE) in single microbial fuel cells. *Environ. Sci. Technol.* **2006**, *40*, 364−369.

(6) Katz, E.; Willner, I. Probing biomolecular interactions at conductive and semiconductive surfaces by impedance spectroscopy: Routes to impedimetric immunosensors, DNA-sensors, and enzyme biosensors. *Electroanalysis* **2003**, *15*, 913−947.

(7) Barsoukov, E.; Macdonald, J. R. *Impedance Spectroscopy Theory, Experiment, and Applications*, 2nd ed.; Wiley-Interscience: Hoboken, NJ, 2005.

(8) Katz, E.; Willner, I. A biofuel cell with electrochemically switchable and tunable power output. *J. Am. Chem. Soc.* **2003**, *125*, 6803−6813.

(9) Rabaey, K.; Lissens, G.; Siciliano, S. D.; Verstraete, W. A microbial fuel cell capable of converting glucose to electricity at high rate and efficiency. *Biotechnol. Lett.* **2003**, *25*, 1531−1535.

(10) Liu, H.; Ramnarayanan, R.; Logan, B. E. Production of electricity during wastewater treatment using a single chamber microbial fuel cell. *Environ. Sci. Technol.* **2004**, *38*, 2281−2285.

(11) Oh, S.; Logan, B. E. Hydrogen and electricity production from a food processing wastewater using fermentation and microbial fuel cell technologies. *Water Res.* **2005**, *39*, 4673−4682.

(12) Min, B.; Kim, J.; Oh, S.; Regan, J. M.; Logan, B. E. Electricity generaton from swine wastewater using microbial fuel cells. *Water Res.* **2005**, *39*, 4961−4968.

(13) Moon, H.; Chang, I. S.; Kim, B. H. Continuous electricity generation from artificial wastewater using a mediator-less microbial fuel cell. *Bioresour. Technol.* **2006**, *97*, 621−627.

(14) Angenent, L. T.; Karim, K.; Al-Dahhan, M. H.; Wrenn, B. A.; Domiguez-Espinosa, R. Production of bioenergy and biochemicals from industrial and agricultural wastewater. *Trends Biotechnol.* **2004**, *22*, 477−485.
(15) Logan, B. E. Biologically extracting energy from wastewater: Biohydrogen production and microbial fuel cells. *Environ. Sci. Technol.* **2004**, *38*, 160A−167A.
(16) Angenent, L. T.; Sung, S. Development of anaerobic migrating blanket reactor (AMBR), a novel anaerobic treatment system. *Water Res.* **2001**, *35*, 1739−1747.
(17) Clesceri, L. S.; Greenberg, A. E.; Eaton, A. D. *Standard Methods for the Examination of Water and Wastewater*, 20th ed.; American Public Health Association: Washington, DC, 1998.
(18) Katz, E.; Filanovsky, B.; Willner, I. A biofuel cell based on two immiscible solvents and glucose oxidase and microperoxidase-11 monolayer-functionalized electrodes. *New J. Chem.* **1999**, *23*, 481−487.
(19) Wagner, N. Characterization of membrane electrode assemblies in polymer electrolyte fuel cells using a.c. impedance spectroscopy. *J. Appl. Electrochem.* **2002**, *32*, 859−863.
(20) Liu, H.; Cheng, S.; Logan, B. E. Production of electricity from acetate or butyrate using a single-chamber microbial fuel cell. *Environ. Sci. Technol.* **2005**, *39*, 658−662.
(21) Rabaey, K.; Boon, N.; Siciliano, S. D.; Verhaege, M.; Verstraete, W. Biofuel cells select for microbial consortia that self-mediate electron transfer. *Appl. Environ. Microbiol.* **2004**, *70*, 5373−5382.
(22) Oh, S. E.; Min, B.; Logan, B. E. Cathode performance as a factor in electricity generation in microbial fuel cells. *Environ. Sci. Technol.* **2004**, *38*, 4900−4904.
(23) Bard, A. J.; Faulkner, L. R. *Electrochemical Methods: Fundamentals and Applications*, 2nd ed.; John Wiley & Sons: New York, 2001.

Received for review February 18, 2006. Revised manuscript received May 9, 2006. Accepted May 24, 2006.

ES060394F